Nonlinear Systematic Distortions Compensation in Satellite Images Based on an Equivalent Geometric Sensor Model Recovered From RPCs

Hui Cao, Pengjie Tao, Yuxuan Liu, and Haihong Li

***Abstract*—The rational polynomial function is widely accepted as the preferred sensor model for high-resolution satellite imagery (HRSI). However, satellite images and their associated rational polynomial coefficients (RPCs) often suffer from nonlinear systematic errors, which were caused by attitude oscillation, sensor deformation, and many other imperfect calibration errors, thus affecting the geo-referencing accuracy. Instead of modeling the biases by polynomials in the image space or refining RPCs directly, this study proposes an approach of going back to the physical model and correcting the local distortions in a self-calibration block adjustment. The algorithm of an equivalent geometric sensor model (EGSM) recovery from RPCs is described in detail. As an equivalent form of the physical sensor models, EGSM reflects the complete viewing geometry of push-broom HRSI. The interior and exterior orientation parameters of EGSM can be stably recovered from RPCs without using any metadata. An approach of RPCs refinement by self-calibration block adjustment based on EGSM is introduced. This approach can effectively compensate for the nonlinear systematic errors caused by platforms and sensors similar to the approach of a rigorous sensor model. The performance of EGSM-based block adjustment is compared with the RFM-based bias compensation method. Experiments using ZY-3 images show the EGSM-based approach can effectively eliminate the nonlinear distortions in satellite images caused by sensor deformation and attitude vibrations. Furthermore, experiments using images from various satellites show that the original RFM can be well fitted with the EGSM and the residuals are smaller than 0.1 pixels for all test images.**

***Index Terms*—Equivalent geometric sensor model (EGSM), high-resolution satellite imagery (HRSI), nonlinear systematic distortions compensation, refinement of RPCs, sensor modeling.**

I. Introduction

SATELLITE images with the rational polynomial coefficients (RPCs) released by vendors generally have certain direct positioning accuracy and can be used in digital surface model matching, orthophoto generation, stereo mapping, and other applications. However, the limited accuracy of orientation measurements, imperfect calibration parameters, and high-frequency attitude vibrations of satellite platforms lead to significant nonlinear systematic errors in satellite images and their associated RPCs. Previous studies have shown that most modern satellite sensors suffer from local distortions, such as Pleiades [1], WorldView-2 [2], Cartosat-1 [2], MappingSatellite-1 (TH-1) [3], ZY-3 [2], [4]–[7], and Yaogan-26 [6]. The systematic errors directly lead to some difficulties in eliminating the y-parallax of satellite imagery in the application of stereo mapping and image matching. Moreover, the nonlinear distortions result in the presence of artifacts in 3-D coordinates of object points derived from images and consequently the reduced quality of related products.

To effectively eliminate the nonlinear systematic errors in satellite images, a block adjustment or imagery orientation based on an appropriate sensor model has to be conducted. The sensor model used in the block adjustment consists of three primary components: a ground-to-imagery mapping function, a set of adjustable parameters affecting the function, and an error covariance corresponding to the observation errors.

The sensor modeling of high-resolution satellite imagery (HRSI) is generally divided into two types: rigorous geometric sensor models (RSMs) and rational function models (RFMs) [7]–[11]. RSMs reflect the physical reality of the complete viewing geometry and correct distortions caused by platform vibration, sensor calibration, Earth rotation, satellite motion, atmospheric refraction, and sometimes deformations of map projection [12]–[14]. The implementation of RSMs requires observations (such as satellite ephemeris, attitude, and sensor structure) on the satellite platforms and sensors. The necessary data is typically not fully released by vendors [10], making it hard in practice to use RSMs for the orientation of satellite images [8], [13]. RFMs represent the ground-to-imagery relationship of RSMs as rational polynomials that map the coordinates of a 3-D ground point to a 2-D image point. Even though it is an approximation of the RSM, the RFM hides various details associated with the specific satellite platform and sensor, thus contributing to the proprietary sensor development. RFMs have been widely applied for almost all modern high-resolution satellite sensors [8], [15]–[17] so that RPCs have become standard release data for HRSI nowadays.

Despite the advantages of RFMs, it is hard to directly optimize the RPCs within a least-square framework due to strong

Manuscript received November 19, 2020; revised February 19, 2021, August 23, 2021, and October 17, 2021; accepted November 19, 2021. Date of publication November 23, 2021; date of current version December 8, 2021. This work was supported in part by the National Natural Science Foundation of China under Grant 41971420 and in part the National Basic Surveying and National Key R&D Program of China under Grant 2018YFD1100405. *(Corresponding author: Pengjie Tao.)*

The authors are with the School of Remote Sensing and Information Engineering, Wuhan University, Wuhan 430079, China (e-mail: huicao@whu.edu.cn; pjtao@whu.edu.cn; yxliu@casm.ac.cn; haihong.lee@qq.com).

Digital Object Identifier 10.1109/JSTARS.2021.3130072

correlations between the parameters [8]–[11], [18]–[20]. It is of great theoretical significance and practical value to develop geometric sensor models with a set of adjustable parameters that can be fully recovered from RPCs and then be used in block adjustment to represent and analyze local image distortions caused by various systematic errors. The general form of the equivalent geometric sensor model (EGSM) was introduced and the EGSM-based approach of block adjustment with DEM as controls was presented for accurate geo-referencing stereo satellite images [21]. The performance was verified with various publicly accessible digital elevation models (SRTM, AW3D30, and ASTER GDEM) as additional or exclusive controls. It was stated that the initial values of the EGSM's parameters can be completely recovered from the RPCs [21]. However, how to get the initial values or establish the EGSM of satellite imagery with the associated RPCs was not discussed there.

In this study, the EGSM is formulated as a specific physical sensor model associated with three very general assumptions (common senses) of a perfect push-broom sensor, and then it is further expressed as a well-known time-dependent collinearity equation in the orbital-attitude format of RSMs. Similar to RSMs, the model parameters of an EGSM have clear geometric interpretations. They consist of the focal length, principal point offset, projection centers of image lines (orbit positions), and the instantaneous attitude of the platform and sensors. With appropriate definitions of the orbital and sensor space coordinates systems, all of the model parameters can be stably recovered from the RPCs of HRSI without using any metadata of the satellite platform or sensor, step by step. The effectiveness of the method is verified using experimental datasets from various satellite sensors.

To illustrate the enhancements of EGSM for compensation of nonlinear systematic errors, an approach of EGSM-based self-calibration block adjustment of multiview satellite images for RPCs optimization is presented and verified. Comparative experiments of bundle adjustment based on EGSM and RFM prove the excellent performance of the EGSM approach.

The rest of this article is organized as follows. Section II reviews the related works. Section III illustrates the nonlinear systematic errors of multiview satellite images and their impact on the ground coordinates obtained from the intersection of stereo models. Section IV introduces the algorithms and steps of EGSM recovery from RPCs in detail. Section V addresses the self-calibration bundle adjustment based on EGSM. Then, the experimental results, analysis, and discussions are presented in Section VI. Finally, Section VII concludes this article.

II. Related Works

The RPCs provided by satellite image vendors are usually derived from the RSMs without using ground control information. The inherent biases of satellite orbit and attitude are introduced into the RPCs, therefore influencing the orientation accuracy of the images. While additional control information becomes available, the RFMs can be optimized directly or indirectly [22]. The indirect refining methods introduce a set of adjustable parameters of the complementary polynomials in the image or object space and keep the original RPCs remain unchanged, while the direct refining methods update the constrained version or subset of the original RPCs within an optimization framework. The optimization can be conducted for single imagery or a block of multiple images. The tie-points extracted from multiple images can be incorporated in the block adjustment, and the stereo-models can be refined resulting in better relative geometric consistency between images and better accuracy of the geo-referencing results [8], [23]. The approaches based on geometric parameters extracted from RPCs can also be classified as direct methods of RPC refinement because they directly modify the RPCs.

The potential for recovering RSM parameters from the RPCs was reported by Di *et al.* [24]. The approach was performed in two steps. The exterior orientation (EO) parameters of the two end image lines from the RPCs were computed first by space resection to initial the EO polynomials. Then the interior orientation (IO) parameters and EO polynomial coefficients were estimated through a bundle adjustment using the 3-D virtual control points (VCPs) generated from the RPCs. Experiments prove the feasibility of this method on the airborne high-resolution stereo camera, but the RPCs of IKONOS images are not sufficient to solve the orientation parameters of the RSM.

High-resolution satellite sensors always have a long focal length and small viewing angle. And the topographic relief is mostly much smaller compared to the satellite's flying height. These configurations lead to a strong correlation between RSM's parameters [7], [9], [10]. It is hard to obtain stable results by simply using the traditional space resection methods to simultaneously solve all IO and EO parameters of an RSM.

A generic method for RPCs refinement and local distortions compensation was proposed by Xiong and Zhang [25]. A light ray is created based on the image coordinates of the GCP and RPCs, and the sensor's pseudo position is restored by the extension of this line to a fixed flight height. Then the pseudo attitude is obtained by the tilted angles of this light ray in the object coordinates system. Adjustment observation equations are constructed for each GCP based on the restored pseudo position and attitude. Experiments show the method yields highly accurate results under a variety of different sensor positions and attitude errors [25], [26]. A calibration method for nonlinear distortions compensation and new RPCs generation was proposed by Huang *et al.* [27]. A procedure of separate recovery of satellite positions and attitudes from RPCs was briefly introduced. Experiments using the wide-view sensor of GF-1 images show that the orientation accuracy improved to about 1 pixel with an appropriate configuration of GCPs [27].

It is known that the simultaneous determination of the RPCs is an ill-posed problem [15], [18], [20]. Some direct methods resolve the problem through the use of parameter selection strategies, such as estimation based on scatter matrix and stepwise regression [18] and optimization based on principal component analysis [20], to update only a subset of the original RPCs, whereas the regularization-based methods try to optimize a constrained version of RPCs, such as the L1-norm minimization [19], the incremental discrete Kalman filtering [22], the batch iterative least squares, and the sequential least squares [24].

A number of indirect methods have been proposed and studied for refining the RFMs of satellite images to compensate for local distortions and improve geo-referencing accuracy.

The high-frequency attitude data measured by special instruments [6] or massive image processing [4], [28] is applied to recover the high-frequency attitude oscillation and then compensate for the platform jitter. Higher-order functions, such as high-order polynomials [29], thin-plate smoothing splines [30], and cubic splines [5], are used to model the local distortions and have achieved satisfactory results. An approach was proposed by Tong *et al.* [4] for the detection of periodic image distortions of ZY-3 caused by attitude oscillation in the across-track direction. The relative distortions are detected by using the back-projected residuals of a large number of tie-points between the stereo images. The sum of sinusoidal functions is estimated with the steepest descent algorithm. The experimental results showed that the discrepancies of ZY-3 images were reduced to a half-pixel level after distortion compensation. In the approach proposed by Cao *et al.* [5], first the RPCs are calculated using a three-dimensional VCPs grid generated by a rigorous physical sensor model, and then, the cubic splines coefficients are solved to model the residual errors of the VCPs. The RFM-based imagery orientation of this approach has achieved satisfactory results for ZY-3 [5]. The thin-plate spline was adopted in an RFM bias-compensation approach to correct nonlinear distortions of vendor-provided RPCs by Shen *et al.* [30]. The performance of this method was evaluated by the use of ZY-3 images and compared against the affine transformation and quadratic-polynomials based methods. The experimental results demonstrated that the thin-plate spline was more effective at removing the systematic bias of the ZY-3 images when more GCPs are used [30].

It has been proved that the bias-compensation methods are effective only when the bias of satellite position and attitude is small, the sensor's field-of-view is narrow, and there are no high order distortions in the images [10], [23], [25], [27]. Besides, refined geo-positioning results always need to refer to the bias correction parameters. This may result in an awkward situation when the correction parameters could not be adopted by the existing software systems. Therefore, RPCs modification or regeneration has to be conducted to incorporate the bias correction parameters into the original vendor-supplied RPCs [27], [29].

III. Nonlinear Systematic Errors of Satellite Images and Their Impacts on Block Adjustment

Although satellite platforms and sensors undergo rigorous laboratory calibration before launch, the calibration parameters change due to various external and environmental forces during launch and on-orbit flight. HRSI vendors usually perform on-orbit calibration for the satellite platforms and sensors during the initial stage of launch and subsequent operations. A set of calibration parameters is calculated to compensate for known systematic errors and provide sensor-calibrated imagery products to users. However, in many cases, the provided satellite images and associated RPCs still have obvious systematic errors.

A region of approximately 100 km $\times$ 100 km in the west of Beijing, China is used for tests to illustrate the systematic errors of satellite images. The area covers a broad range of typical terrain types, including flat land, hills, and mountains.

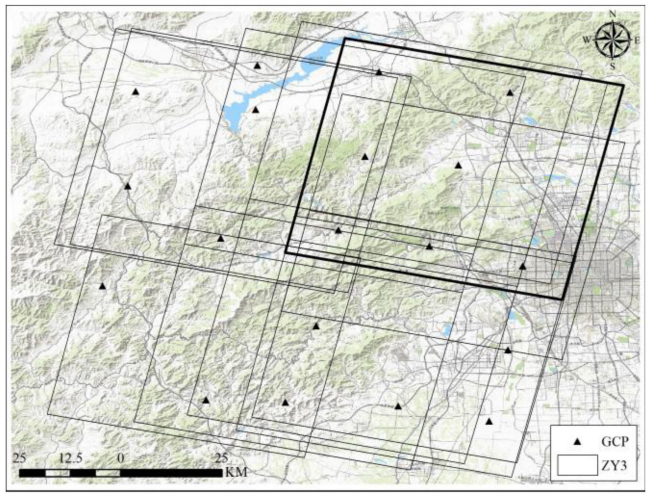

Fig. 1. Distribution of ZY-3 images and GCPs near Beijing, China.

TABLE I
RFM-Based Block Adjustment Results of ZY-3 Images (Unit: m)

Number of GCPs	Mean error			Standard deviation				RMSE	
	X	Y	Z	X	Y	XY	Z	XY	Z
0	0.3	11.2	7.7	2.4	1.5	2.8	2.3	11.6	8.0
1	–0.6	–0.7	1.2	2.4	1.5	2.8	2.3	3.0	2.6
4	1.6	–0.6	–0.9	2.1	1.2	2.4	1.6	2.9	1.9
5	1.1	–0.6	–0.5	2.1	1.2	2.4	1.6	2.7	1.7
8	0.4	–0.3	–0.5	1.9	1.1	2.2	1.7	2.3	1.8
9	0.2	–0.3	–0.3	1.9	1.1	2.2	1.7	2.3	1.7
19	0.0	0.0	0.1	1.8	1.1	2.1	1.4	2.1	1.4

The test images are 36 ZY-3 sensor-calibrated level-1 products with RPCs, captured between February 2012 and January 2015. The 36 images make up 12 stereo models, each of them consists of three images captured separately by the forward, nadir, and backward cameras, whose ground sampling distances (GSDs) are about 3.5, 2.1, and 3.5 m, respectively. The forward and backward cameras have view angles of about $\pm 22^\circ$ to the nadir camera, forming a base-height ratio of 0.81. A total of 19 well-distributed remarkable GCPs are used as control data or check-points for the assessment of adjustment accuracies. The distribution of the test images and GCPs is shown in Fig. 1.

The GCPs are collected by the GPS-RTK survey. The geodetic datum is the WGS84 reference system and the elevation is geodetic height. The accuracies of the object coordinates are better than 0.1 m. The image point coordinates of these GCPs are manually measured in a 3-D environment, and the accuracy of image point measurements is better than 0.5 pixels. Approximately 40 000 tie points are automatically extracted by multilevel image matching and there are about 5700 points per image. More than 60% of the tie points are located in four or more images. RFM-based block adjustments with a set of affine transformation parameters in the image space for bias compensation are carried out. Different numbers of GCPs are used and whose a priori planimetric and height accuracy is set to 2.0 and 1.0 m, respectively. The root mean square error (RMSE), mean and standard deviation of the object coordinate residuals are counted and shown in Table I.

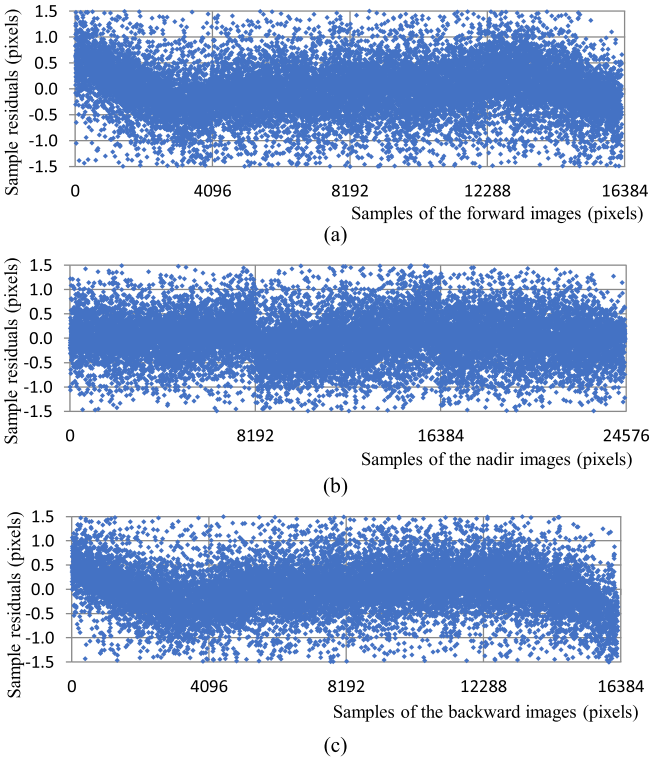

Fig. 2. Residuals distribution of image points along the scanning line (unit: pixel): the sample coordinate residuals v_s of (a) forward, (b) nadir, and (c) backward imagery along their CCD line.

Through the coordinate residuals of the ground checkpoints, it can be seen that the main factor affecting positioning accuracy is the translations contained in the RPCs. When using one control point to eliminate the shifts, the absolute positioning accuracy is greatly improved. When more control points are used, the accuracy continues to improve but not significantly. The residual errors (v_l, v_s) of image coordinates of a tie-point are derived from the observation equations of the RFM-based block adjustment [7], [8], [15]. They are computed for every image point after the block adjustment by the adjusted ground coordinates of the tie-points and the adjusted affine transformation parameters of the satellite images. The local distortions or nonlinear systematic errors of the image coordinates are analyzed in detail below based on the residuals.

A. Deformation of the Linear Array CCD

The image coordinate residuals (v_l, v_s) in seven of the 12 stereo scenes have a similar distribution along the image row (the scan line). For better visualization, the residuals of three scenes are merged and presented for the forward, nadir, and backward imagery in Fig. 2, respectively. The CCD arrays of forward, nadir, and backward imagery of the ZY3 satellite are composed of 4, 3, and 4 detector elements. The CCD segment is visible in Fig. 2, the segments of the residual's distribution are well consistent with the components of CCD arrays. It can be easily understood that the CCD array has obvious systematic deformation. The deformation near the ends of the CCD lines reaches 0.6 pixels.

B. Nonlinear Systematic Errors Caused by the Jitter of the Satellite Platform

Among the 36 images in the experimental area, the image coordinate residuals (v_l, v_s) of 33 images show a very regular oscillation with amplitude greater than 0.2 pixels along the direction of the image column (the flight direction). The residuals of one image in the upper right corner of the area (marked with bold lines in Fig. 1) are shown in Fig. 3. The systematic oscillation of v_s with respect to the lines of the image can be understood as the high-frequency jitter of the roll angle. It has a frequency of $\sim$0.6 Hz and an amplitude of $\sim$0.2 to 1 pixel, which is consistent with the results of the jitter analysis of the ZY-3 images in [4]. The oscillation of v_l with respect to the line number can be understood as the jitter of the satellite pitch. Its frequency is $\sim$0.2 Hz and amplitude of $\sim$0.2 to 0.4 pixels.

C. Influence of Nonlinear Systematic Error on Coordinates From the Intersection of Stereo Models

The forward intersection is carried out for every stereo model to obtain the 3-D ground coordinates of the tie points by using the bias-compensation parameters from the block adjustment and RPCs of the images. Then these ground coordinates are compared with those of the block adjustment results. The difference shows that the ground coordinates of the stereo models are affected by the local distortions or nonlinear systematic errors of RPCs. While the image coordinate residuals (v_s, v_l) have evident nonlinear systematic errors, the corresponding ground coordinates from the forward intersection of a stereo model systematically differ from the block adjustment results. The coordinate differences of longitude, latitude, and height of the stereo scene in the upper right corner of the area are shown in Fig. 4. They are well related to the image coordinate residuals (v_s, v_l) shown in Fig. 3 where the residuals reflect the unmodeled local distortion which directly affects the ground coordinates of the stereo model intersection. In other words, even with the results of a block adjustment, the unmodeled systematic errors by RPCs and bias-compensation parameters still lead to difficulty in stereo mapping and image matching, resulting in decreased positioning accuracy.

It is worth noting that the RFM-based block adjustment of this example is carried out with a set of affine transformations in the image space for bias compensation. Because the local distortions are not modeled or eliminated by the adjustment, they remained as the residual errors of the image coordinates of the tie-points. However, the accuracy of the ground coordinates is satisfactory on the statistics of the ground check-points. That is an advantage of the block adjustment with multiview images. It is that block adjustment with multiview images is able to decrease the influence of nonlinear systematic errors on the ground coordinates to some extent. In other words, the block adjustment of multioverlapped images produces more robust and consistent results since tie-points between multiple images are incorporated in the process.

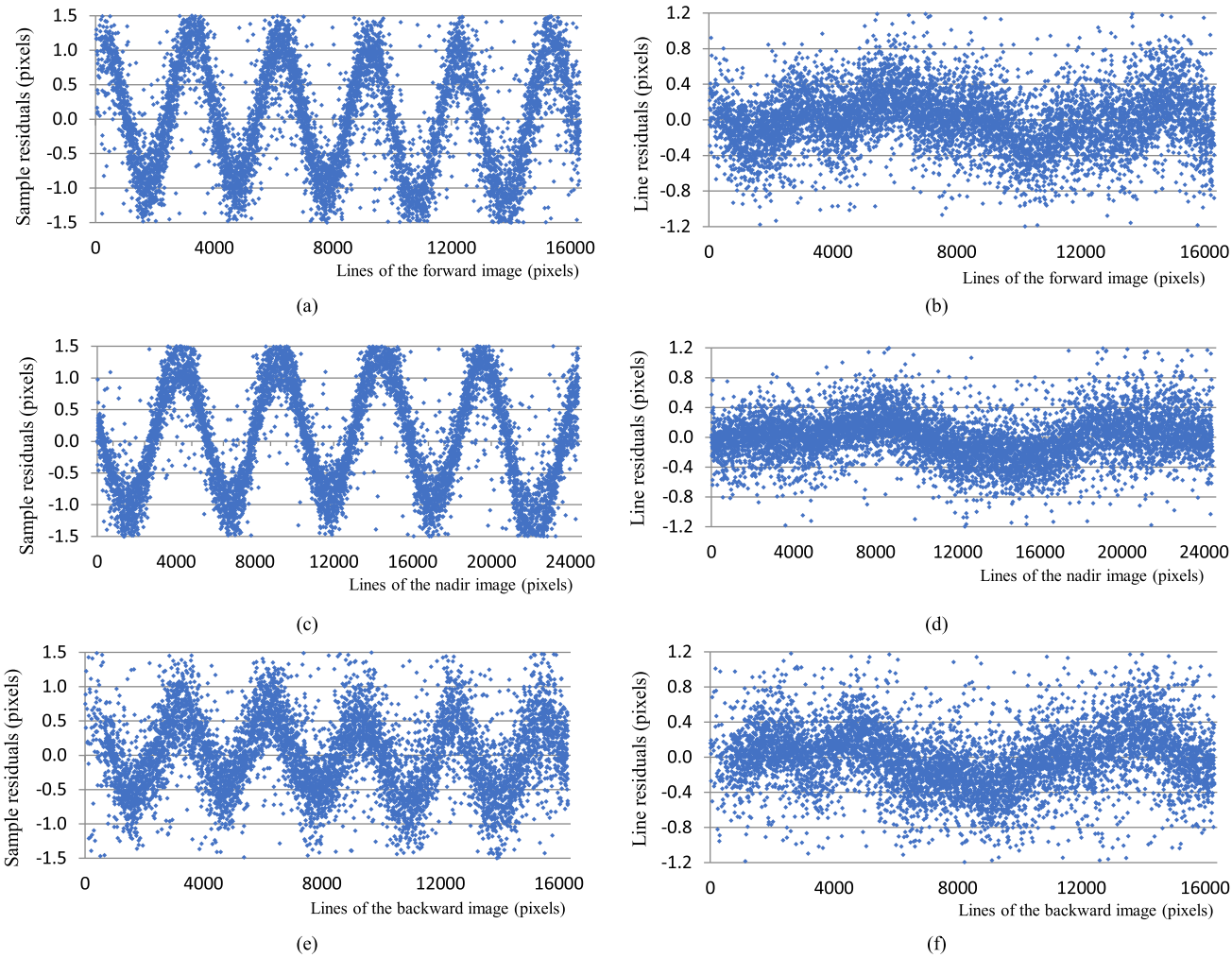

Fig. 3. Residuals undulation of the RFM-based block adjustment (unit: pixel). (a) $\boldsymbol{v_s}$ and (b) $\boldsymbol{v_l}$ with respect to the line of the forward image, (c) $\boldsymbol{v_s}$ and (d) $\boldsymbol{v_l}$ with respect to the line of the nadir image, (e) $\boldsymbol{v_s}$ and (f) $\boldsymbol{v_l}$ with respect to the line of the backward image.

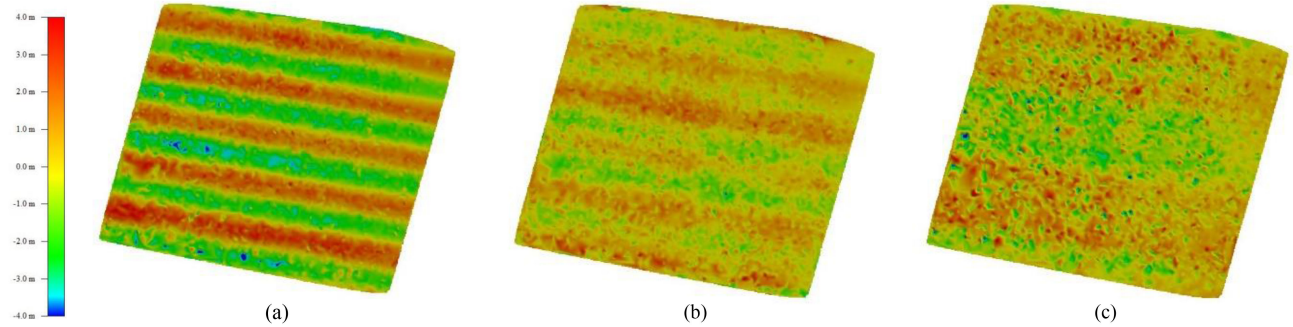

Fig. 4. Differences of ground coordinates between the stereo model intersection and RFM-based block adjustment: residuals in the (a) east-west (longitude), (b) north-south (latitude), and (c) height directions.

IV. EGSM and Parameters Recovery From RPCs

A. RSM of Linear Array Push-Broom Satellite Images

Every satellite platform may have a different mathematical representation of its sensor model, according to the physical properties of its orbit and attitude [9]. This is because each satellite has its orbital reference frame and attitude rotation style [31]. They are usually formulated in an inertial system by a set of coordinate transformations. The RSMs developed mainly in the photogrammetric community are based on the modified or

extended collinearity equations in which the satellite position and rotation about a 3-D coordinate system in object space are referred to as model parameters [7], [8], [13].

The general form of the so-called orbital-attitude physical sensor model [9] is expressed as follows:

$$\begin{bmatrix} -x_0 \\ s - y_0 \\ -f \end{bmatrix} = \lambda \cdot \boldsymbol{R}_s(l) \cdot \boldsymbol{R}_o(l) \begin{bmatrix} X - Xs(l) \\ Y - Ys(l) \\ Z - Zs(l) \end{bmatrix}. \quad (1)$$

Here, $lambda$ is a scale factor, $[l, s]$ is the pixel coordinate (l for line, s for sample) of an image point, x_0 and y_0 is the pixel coordinate of the principal point, and f is the equivalent focal length (all in pixels). The instantaneous position of the projection center corresponding to the scan line l is described by *Xs*(*l*), *Ys(l)*, and *Zs(l)*, which can be calculated by the orbit equation or orbital elements. The instantaneous rotation matrix $\boldsymbol{R}_o$ *(l)* represents the transformation from the GRS to the orbital reference frame, expresses the instantaneous attitude of the orbital coordinate system of the satellite platform relative to the GRS. It can be calculated by the instantaneous position and velocity vector (the first derivative of the orbit equation) of the satellite. The $\boldsymbol{R}_s$ *(l)* is the rotation matrix of the orbital reference system to the sensor frame, which expresses the rotation between the image coordinate system and the orbital reference frame of the satellite platform, for example, the offset angle of the forward and backward viewing cameras, the roll angle of a side-viewing camera, or the pointing angles of an asynchronous (agile satellite) sensor, etc. The parameters of an RSM consist of IO parameters *f,* x_0 and y_0, and EO parameters *Xs(l)*, *Ys(l)*, *Zs(l)*, rotation angles of $\boldsymbol{R}_o$ *(l)* and $\boldsymbol{R}_s$ *(l)*.

The main obstacle to the implementation of such a general RSM is that the necessary parameters are not always completely provided in the metadata file, or they are not accessible at all [10].

B. EGSM and Its Parameters Recovery From RPCs

To avoid the dependence of the geometric sensor model on the sensor's configurations and metadata, an EGSM is proposed based on the following mathematical assumptions [21].

1) The ideal linear array CCD is placed on the focal plane of the camera as a straight line with the same pixel size. Its conformation corresponds to a row of the satellite imagery.
2) Each row of a push-broom HRSI is acquired by a perspective projection.
3) During the short imaging time, the satellite's motion around the Earth is very smooth. The sensor's position and attitude can be represented as a set of polynomials of the time or rows of the imagery.

With these assumptions, the EGSM can be understood as the geometric model of a perfect push-broom sensor. It is expressed in the same format of RSMs as (1), which defines the instantaneous position of the projection center in an earth-fixed GRS (WGS84) and defines the attitude of the satellite platform and sensors separately. This allows the EGSM parameters can be completely and stably recovered from the RPCs without using any metadata regarding the platform or sensor structure. At the same time, the geometric meaning of the model parameters is more directly interpretable, therefore, more convenient to introduce additional constraints on the parameters. The collinearity equations of the image point, the projection center, and the object point established on this basis are completely equivalent to the RSMs from a mathematical point of view.

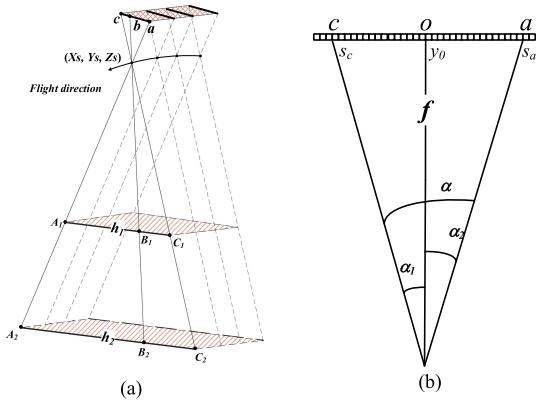

Fig. 5. Sensor geometry for EGSM recovery from RPCs of satellite images. (a) Sensor geometry of a scan line. (b) Relationship between the focal length and principal point.

The EGSM parameters in (1) consist of *f*, x_0 y_0, *Xs(l)*, *Ys(l)*, *Zs(l)*, and independent rotation angles in the matrix $\boldsymbol{R}_o$ *(l)* and $\boldsymbol{R}_s$ *(l)*. To avoid the high correlation between the orientation parameters and ensure the stability of the calculation, instead of using space resection or bundle adjustment to solve all of them simultaneously [24], the IO parameters, projection centers, and rotation angles of an EGSM are separately recovered from RPCs step by step according to the geometric properties of the parameters. It is noteworthy that the establishment of the EGSM does not require any other information except for the RPCs of the satellite imagery, which ensures the universality of the model. The steps and algorithms of the EGSM parameters recovery are discussed in detail as follows.

1) Line of Sight Constitution Based on RPCs: The general expression of the RFM is as follows [7], [15]:

$$\begin{cases} L = \mathrm{Num}_l(e,n,h) / \mathrm{Den}_l(e,n,h) \\ S = \mathrm{Num}_s(e,n,h) / \mathrm{Den}_s(e,n,h) \end{cases}. \quad (2)$$

Here, *(L,S)* are the normalized image coordinates, and *(e,n,h)* are the geodetic coordinates of a ground point. The *Num(e,n,h)* and *Den(e,n,h)* are cubic polynomials (including normalization operations). The 80 RPCs and the ten normalized parameters are referred to as RPCs, which are provided to the user along with the satellite images.

Given the pixel coordinates *(l,s)* of an image point, its normalized coordinates are calculated as follows:

$$\begin{cases} L = (l - \mathrm{line\_offset}) / \mathrm{line\_scale} \\ S = (s - \mathrm{sample\_offset}) / \mathrm{sample\_scale} \end{cases}. \quad (3)$$

Given a ground height h to the image point, the longitude and latitude *(e,n)* of the corresponding object point can be obtained by iterations of (2). The geodetic coordinates *(e,n,h)* can be converted into *(X,Y,Z)* in the GRS.

As shown in Fig. 5, for the selected image point *a(l,s_a)* on a scan line. Given the maximum height h_1 and minimum height

h_2 expressed by RPCs (the height offset and scale), the object coordinates of points A_1 and A_2 corresponding to image point a can be obtained based on the above algorithms. The virtual line of sight $\overrightarrow{A_1A_2}$ is constituted for image point *a*. It is noteworthy that the line of sight obtained from RPCs is different from the actual one by which the image point was acquired due to the atmospheric refraction and other distortions. This line of sight does represent the collinearity property of a perfect sensor for the image point, the projection center, and the corresponding object point. This is the basis of sensor geometry for EGSM parameters recovery from the RPCs of satellite images.

2) Recovery of the Focal Length and Principal Point Offsets: Without loss of generality, one can set $x_0 = 0$ for a linear array sensor. As shown in Fig. 5(b), the image point $c(l, s_c)$ is an image point of the scan line and $a(l,s_a)$ is another point on the same row. Based on the first assumption of EGSM and the sensor geometry showed in Fig. 5, one can simply get $\tan(\alpha_1)=(y_0 - s_c)/f$ and $\tan(\alpha_2) = (s_a - y_0)/f$. Then the angles between the lines of sight in image space satisfy the following equation:

$$\tan(\alpha) = \frac{f * (s_a - s_c)}{f^2 + (s_c - y_0) * (s_a - y_0)}. \tag{4}$$

Referring to Fig. 5(a), α is the angle between straight lines $\overrightarrow{A_1A_2}$ and $\overrightarrow{C_1C_2}$ in object space and $\tan(\alpha)$ can be calculated by vector operations with their object coordinates. For the image point $b(l,s_b)$, the other two similar equations can be created. By using these three equations (two of them are independent), the quadratic terms can be eliminated and the initial values of f and y_0 can be obtained. To ensure the stability and accuracy of the solution, multiple scan lines can be selected in the image and multiple image points can be used on every scan line. Then, a set of observation equations can be formed according to (4). The optimal values of f and y_0 can be solved by a least-squares adjustment.

3) Recovery of the Projection Center of a Scan Line: In EGSM the imaging geometry of each scan line of an image is a perspective projection, therefore, the projection center of the scan line is the intersection of lines of sight of image points on that row. As shown in Fig. 5(a), the object coordinates and lines of sight of image points $a(l, s_a)$ and $b(l, s_b)$ on the scan line can be calculated by the algorithm described in step (1). Then, four equations can be obtained for straight lines $\overrightarrow{A_1A_2}$ and $\overrightarrow{B_1B_2}$ in the 3-D space. The intersection of these two straight lines is the projection center. By solving the equations, the projection center's coordinates (X_s, Y_s, Z_s) can be obtained.

Multiple image points on the row should be used to ensure the stability of the solution. As an HRSI camera has always a small viewing angle, this may affect the accuracy and stability of intersection computation. The constraints of angles between lines of sight discussed in step (2) can be integrated with the observation equations of the straight lines to improve the intersection accuracy and ensure the consistency of the projection position and the IO parameters. Then the 3-D coordinates of the projection center $Xs(l)$, $Ys(l)$, and $Zs(l)$ of a scan line can be computed by a least-squares adjustment. By using the lines of sight and their geometric relationship, the position of the project center of any scan line of HRSI can be stably obtained.

4) Polynomials Fitting of the Satellite Trajectory: A series of Keplerian orbital elements are often combined to model the real satellite trajectories affected by gravitational perturbations and relativistic effects. To reduce the computational complexity, improve the computational stability and efficiency, the interpolation of a polynomials' fitted orbit can be used [32]. In this study, *n*th-order Chebyshev polynomials are used for fitting the position of projection centers. In an image scene, m lines $(m > n)$ are selected as the reference lines, and their projection centers' object coordinates can be computed from RPCs based on the algorithm discussed in Section IV-B). The polynomial fitting is further solved by the least-squares methods. Then for any scan line in the image, the object coordinates of its instantaneous orbit position and the velocity vectors of the satellite can be calculated using *n*th-order Chebyshev polynomials. Previous studies show that an orbit section of an image scene can be well fitted by third-order Chebyshev polynomials [21]. This also indicates that RFMs do not represent the high-order terms of attitude oscillations.

5) Instantaneous Rotation of the Orbital Reference System: Based on the fact that the Earth's center is one of the focus points of the satellite's orbit, the orbital reference system can be simply defined by its instantaneous positions and velocity vectors in the GRS. The origin of the orbital reference frame is defined as the instantaneous projection center. The *z*-axis is coincident with the instantaneous position vector, pointing from the Earth's center to the satellite position. The *x*-*z* plane coincides with the plane composed of position and velocity vectors with the x-axis pointing towards the satellite motion and the *y*-axis completing a right-hand system.

Given an image point (l, s), the instantaneous position vector $\vec{p} = (X_s, Y_s, Z_s)$ and the velocity vector $\vec{v} = (v_x, v_y, v_z)$ can be obtained by the orbit polynomials and their first derivatives respectively. Then, the instantaneous rotation matrix $\boldsymbol{R}_{\mathbf{o}}(l)$, i.e., the unit vectors of the orbital reference frame in the GRS can be obtained by vector calculations.

6) Rotation Matrix of the Sensor: When the instantaneous position of the projection center and the rotation matrix of the orbital reference frame are known, the EGSM can be simplified as follows:

$$\begin{bmatrix} 0 \\ s - \mathrm{y}_0 \\ -f \end{bmatrix} = \lambda \cdot \boldsymbol{R}_s(l) \begin{bmatrix} u(l) \\ v(l) \\ w(l) \end{bmatrix}. \tag{5}$$

Here, $[u(l), v(l), w(l)]$ are coordinates of the object point in the orbital reference frame. They can be obtained by the object point coordinates in the GRS (derived by RFM from the image coordinates and given heights), the instantaneous position of the projection center, and the rotation matrix $\boldsymbol{R}_{\mathrm{o}}(l)$.

Based on the EGSM geometry, the sensor's coordinate system can be defined by the linear array CCDs and the principal axis. The origin of the system is defined as the projection center. The *z*-axis is the line of sight of the principal point, i.e., the principal axis. The *x*-axis is coincident with the normal vector of the plane formed by any two lines of sight of a scan line [refer to Fig. 5(a)] and the *y*-axis completing a right-hand system. Therefore, the initial instantaneous rotation matrix $\boldsymbol{R}_s(l)$ can be constructed by vector calculations similar to $\boldsymbol{R}_{\mathrm{o}}(l)$ discussed in step (5).

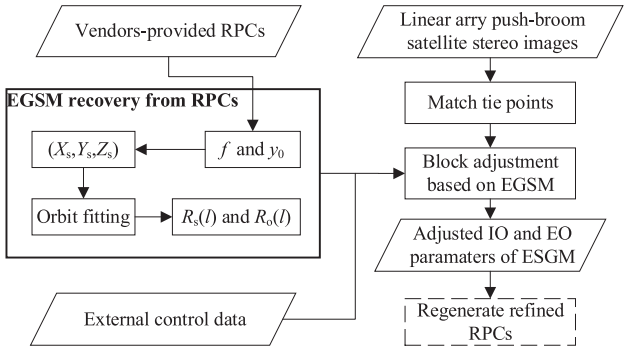

Fig. 6. Workflow of block adjustment based on EGSM.

In this study, a unit quaternion $[q_0, q_1, q_2, q_3]$ is used to express the sensor's attitude, and Chebyshev polynomials are used for the representation of the angular rates w_x, w_y ,w_z of the quaternion update. Multiple scan lines (more than the order of Chebyshev polynomials) are selected for each image scene and multiple image points on each scan line are used as observations. The coefficients of the Chebyshev polynomials of w_x, w_y ,w_z are solved iteratively by a least-squares approach. And the instantaneous rotation matrix $\boldsymbol{R}_s(l)$ can be refined by the updated unit quaternion.

Previous studies showed that the quaternion-based approach for space-resection does not need to provide user-defined approximate values and performs accurately for oblique and vertical images [33]. In this study, the initial value of the unit quaternion is derived from the rotation matrix $\boldsymbol{R}_s(l)$ by a few scan lines of the imagery. Even though the sensor has a large rotation angle, e.g., the pitch angle of the forward and backward view sensors of ZY-3 and TH-1 satellite is about $\pm 25°$, and the off-nadir view angle of WV2 images may be larger than 30°, the calculation always converged in a few iterations.

Based on the algorithms given in this section, EGSM's IO and EO parameters can be completely recovered from RPCs step by step. The correlated parameters are separately solved in different steps to ensure a stable solution. By using the unit quaternion, the convergence can be quickly and stably achieved even when the view angle is large and there is no initial value.

V. RPCs Refinement With Self-Calibration Block Adjustment Based on EGSM

The procedure of block adjustment and RPCs optimization based on EGSM is shown in Fig. 6. The multilevel pyramid image matching method is used to automatically extract the tie points on images and the initial values of the object coordinates of the tie points can be obtained by a multiview intersection. The external control data serves as a geo-reference for bundle adjustment, including GCPs and other generalized control data, such as orthophoto maps and digital elevation models [21].

A. Observation Equations of Tie-Points

The instantaneous position and attitude of a real satellite's orbit deflects over time due to gravitational perturbations by other objects, the effects of relativity, and numerous other disturbances. The systematic errors of image points can be expressed in terms of additional parameters. Considering all these model errors, the general form of block adjustment based on EGSM can be expressed as follows:

$$\begin{bmatrix} 0+\Delta x \\ s-y_0+\Delta y \\ -f \end{bmatrix} = \lambda \cdot \begin{bmatrix} u \\ v \\ w \end{bmatrix} + \boldsymbol{e} \begin{bmatrix} u \\ v \\ w \end{bmatrix}$$
$$= \boldsymbol{R}_s(l) \cdot \left[\boldsymbol{D}_{\mathrm{ori}}(l) \boldsymbol{R}_o(l) \begin{bmatrix} X - Xs(l) \\ Y - Ys(l) \\ Z - Zs(l) \end{bmatrix} + \begin{bmatrix} dXs(l) \\ dYs(l) \\ dZs(l) \end{bmatrix} \right]. \quad (6)$$

Here, $\boldsymbol{e}$ is the term for observation errors. It is usually assumed as a zero-mean Gaussian noise. The u, v, and w are auxiliary coordinates of the object point. The Δx, Δy is systematic error corrections or model errors expressed in the form of additional parameters, the $dXs(l)$, $dYs(l)$, and $dZs(l)$ are offsets of the satellite position due to various disturbances, and $\boldsymbol{D}_{\mathrm{ori}}(l)$ is the influence on the attitude of the satellite relative to the orbital reference system. While the model parameters are completely recovered from RPCs, these three components constitute the unknowns of the self-calibration block adjustment system [21].

After eliminating λ in (6), the observation equations of each image point can be expressed by

$$\begin{cases} -e_{xi} = f * u + \Delta x * w \\ -e_{yi} = (s - y_0) * w + f * v + \Delta y * w \end{cases}, p = \sigma_i^2 / w^2. \quad (7)$$

It is noticed that the w defined here is the slant distance from the projection center to the object point. Because the terrain relief is quite smaller compared to the flight height of a satellite, this distance is almost a constant. The linearization of collinearity equations in the form of (7) is much simpler than that of (6).

B. Additional Parameters for Compensation of Sensor Errors

Because space-borne linear array sensors are usually comprised of a merged combination of individual linear CCD segments, piecewise polynomials are appropriate models of optical system distortions and geometric distortions of the CCD segments. In this study, piecewise linear or quadratic polynomials are implemented

$$\begin{cases} \Delta x = a_{i0} + a_{i1}(s - s_i) + a_{i1}(s - s_i)^2 \\ \Delta y = b_{i0} + b_{i1}(s - s_i) + b_{i1}(s - s_i)^2 \end{cases}, s \in (s_{ib}, s_{ie}). \quad (8)$$

Here, a_i, b_i are additional parameters of the ith segment of the sensor, s_{ib}, s_{ie} are the beginning and ending pixels of the segment, and $s_i = (s_{ib} + s_{ib})/2$ is the middle pixel of the segment.

The nodes of CCD segments can be determined based on the knowledge of the sensor's configuration (e.g., length of the segment, number of segments, etc.) or distribution of the residuals. Then a set of additional parameters is defined for each sensor. While these calibration parameters are obtained from the process of on-orbit calibration, they can be integrated into the adjustment model. The time-invariant systematic biases of the images will be precorrected before adjustment.

C. Geometric Constraints of EGSM Parameters

While the satellite's instantaneous position vector is defined as the z-axis of the orbital reference system, the x and y orbital coordinates of the projection center are always zero, and the z is almost a constant within a short imaging segment. Then, a linear relationship of the position offsets and attitude updates can be easily obtained for object points in the orbital reference system. There exist strong correlations between position offsets and attitude updates in this equation as the terrain relief is much smaller than the satellite's flight height. To reduce the influence of this correlation problem for the block adjustment, two sets of constraints are introduced as pseudo observations as follows:

$$\begin{cases} -e_{xc} = dXs\left(l\right) + Hs * d\varphi\left(l\right), p_{xc} \\ -e_{yc} = dYs\left(l\right) - Hs * d\omega\left(l\right), p_{yc} \end{cases}. \tag{9}$$

Here, Hs is the average flight height of the satellite. The polynomials $d\varphi(l)$ and $d\omega(l)$ are the Euler angles pitch and roll of the attitude updates of the rotation matrix $\boldsymbol{D}_{\mathrm{ori}}(l)$. The weights p_{xc} and p_{yc} are determined according to a priori accuracy estimations of the pseudo observations.

D. Self-Calibration Block Adjustment

The observation equations of EGSM after linearization in matrix form can be obtained as follows:

$$\begin{cases} -\boldsymbol{e}_1 = \boldsymbol{B}_{11}\boldsymbol{X}_1 + \boldsymbol{B}_{12}\boldsymbol{X}_2 - \boldsymbol{l}_1, \boldsymbol{P}_1 \\ -\boldsymbol{e}_2 = \boldsymbol{B}_{21}\boldsymbol{X}_1 - \boldsymbol{l}_2, \boldsymbol{P}_2 \end{cases}. \tag{10}$$

Here, $\boldsymbol{X}_1$ are the additional parameters for systematic error corrections, the coefficients of Chebyshev polynomials of satellite position offsets, and attitude deflections; $\boldsymbol{X}_2$ are the tie points' object coordinates; $\boldsymbol{l}_1$, $\boldsymbol{l}_2$ is the constant term, and $\boldsymbol{P}_1$, $\boldsymbol{P}_2$ is the weight matrix. The first term and the second term of (10) correspond to (7) and (9), respectively.

To reduce the correlation between unknowns and avoid overparameterization, the additional parameters for all sensors and the disturbance terms of the instantaneous position and attitude of the satellite obtained from RPCs should be used as pseudo observations [21]. It should be noted that introducing pseudo observation equations is a quite common treatment in bundle adjustment. It provides the flexibility to properly weigh any participants in the combined block adjustment based on a priori knowledge about their precision. The weights in the block adjustment indicate the contribution of each group of observations. In this study, the variances of the image coordinates of the tie points on each image are estimated by their residuals. The unit weight is assigned to image coordinates on the reference image whose variance is set as ${\sigma_0}^2$. Then the weight factors of other observations are computed as $p_i = {\sigma_0}^2/{\sigma_i}^2$ based on their estimated or a priori variance ${\sigma_i}^2$. The a priori standard deviation is chosen as 20 m and 0.01° (about 100 m on the ground), respectively, for position and attitude. For the additional parameters, they are considered as a quite small distortion with a priori standard deviation of 1.0 pixels. From past experiences in photogrammetry, the combined block adjustment is not sensitive to the assignment of weights, especially, of the pseudo observations in this study.

The number of unknowns of $\boldsymbol{X}_1$ is the sum of the additional parameters for every sensor of the block, the coefficients of Chebyshev polynomials of satellite position offsets and attitude deflections of every image of the block. That is much less than the number of unknowns of $\boldsymbol{X}_2$, which is three times the number of tie points of the block. To facilitate the solution, the $\boldsymbol{X}_2$ is eliminated and a reduced normal system is solved in this study. The object coordinates of the tie points are calculated by a multi-image forward intersection algorithm.

During the iterations of the self-calibration step of the block adjustment, the statistics on residuals of the image coordinates are applied per imagery. While a significant systematic error is indicated for the image, the orders of the Chebyshev polynomials of the attitude deflections of the image are accordingly updated.

E. Regeneration of RPCs

For ease of use, the refined RPCs of satellite images are regenerated by the "terrain-independent" algorithm [15] after EGSM-based self-calibration block adjustment. It should be noted that it is impossible to fit all terms of EGSM by RPCs, such as the high-order terms of the position and attitude polynomials in EGSM (the empirical value provided in this study is more than fourth order) and the segmental deformation of linear CCD expressed by additional parameters.

In this study, a correction grid is created to compensate for the residuals of RPCs fitting when its RMSE is larger than the threshold. The model errors contained in the original RPCs can be effectively eliminated by the optimized RPCs obtained from this approach. The correction grid can be easily used to resample the imagery or correct the coordinates of image points to compensate for the high-frequency systematic errors, thus improving the positioning accuracy of the satellite imagery.

VI. Experiments and Analysis

A. Establishment of EGSM

The images of ZY-301/02, TH-101/02, WorldView-2, and Pleiades satellites are used to evaluate the performance of EGSM recovery from RPCs. They are from different vendors, have different GSDs, and are captured with different imaging modes (synchronous or asynchronous). The details of the test data are given in Table II.

1) EGSM Recovery for Pleiades Images and Comparison With the Metadata: The metadata of Pleiades' Primary product (sensor calibrated images) provides all parameters of a geometric sensor model, which is also called the Perfect Sensor model [34], [35]. To validate the algorithms of EGSM recovery from RPCs, the interior and EO parameters of EGSM recovered from RPCs are compared with those recorded in the metadata file.

The focal length recovered from RPCs is the same as the metadata within the decimal places and the difference is smaller than 0.002 pixels relative to the scale of the image. The mean difference of the principal point offset is –0.4 pixels. This might be caused by the truncation error of the parameters in the metadata.

TABLE II
DETAILS OF THE TEST DATA SETS

Satellite Platform	Number of images	Imaging mode	Imaging time	GSD (m)	Test area details
ZY-3 01	219	SYN	2012/05 –2013/06	3.5/2.1	Located in the east of Turpan, Xinjiang Province, the coverage is about 230 km long from north to south and 420 km wide from east to west. The topographic relief is more than 4 km, the lowest elevation is about −200 m, and the area is about 96,000 km^2.
ZY-3 02	384		2017/03 –2017/12	2.5/2.1	Located in Shandong Province, the coverage is about 420 km long from north to south and 700 km wide from east to west. The area covers a variety of terrains such as plains, terraces, hills, and mountains.
TH-1 01	969		2010/12 –2016/02	5.0	
TH-1 02	1197		2012/09 -2016/03	5.0	
WorldView-2	54	ASYN	2018/06/03 and 2018/07/11	~0.5	Located in the east of Jilin Province, China, and the area is about 4,600 km^2. The images are from 4 WorldView-2 strips, 42 of them are captured on June 3, 2018, and the rest are captured on July 11, 2018.
Pleiades	14		2012/02 –2018/01	~0.5	Three images captured in February 2012 are in Melbourne, Australia. They are Pleiades TRISTEREO sample data release by Airbus. (https://www.intelligence-airbusds.com/en/8262-sample-imagery). The other eleven images are in Hunan, Zhejiang, and Sichuan Province, China.

Note: SYN means synchronous and ASYN means asynchronous.

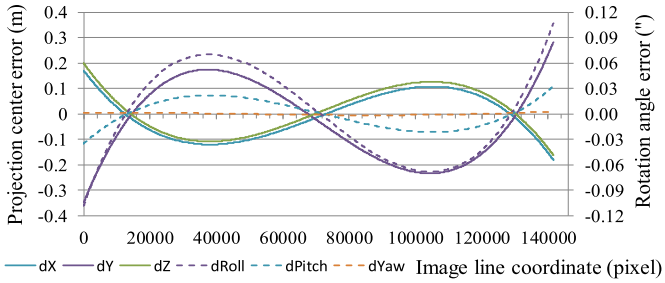

Fig. 7. Differences between EO parameters from metadata and EGSM.

The Pleiades imagery is often cropped according to the user-provided area of interest, the widths of the 14 experiment images are different from 41 425 to 9519 pixels. The IO parameters can be stably recovered from associated RPCs wherever the portion is and even though the image width is smaller than 10 000 pixels (view angles $< 0.4°$).

The satellite position and attitude of every ten rows of an image are calculated by the metadata and the RPCs. The RMSE of the position difference is less than 0.17 m, and that of the attitude is smaller than 0.06 arc-seconds. Considering the GSD of Pleiades imagery is about 0.5 m and the flight height of ~702 km, the difference of the EO parameters is about 0.3 pixels in the image scale. The results of one test image are shown in Fig. 7. The correlation between position and attitude is well demonstrated there.

2) Accuracy of the EGSM Established By RPCs: The equivalent focal length and coordinates of the principal point are calculated for each view type of imagery and the orbit polynomials are obtained by the algorithm described in Section IV. On this basis, the observation equation is set up according to (5) and the rotation matrix of the satellite sensor is calculated by the least-squares adjustment, thus constituting the EGSM of each image. Then, 101 scan lines are evenly distributed on each image, and 101 points evenly distributed on each line are selected.

TABLE III
ACCURACY STATISTICS OF EGSM MODELING RFM (UNIT: PIXEL)

Satellite Platform	Camera	RMSE		Minimum		Maximum	
		Line	Sample	Line	Sample	Line	Sample
ZY-3 01	FWD	0.000	0.001	–0.004	–0.011	0.004	0.011
	NAD	0.000	0.001	–0.004	–0.010	0.004	0.010
	BWD	0.000	0.001	–0.003	–0.010	0.003	0.010
ZY-3 02	FWD	0.002	0.005	–0.023	–0.025	0.022	0.025
	NAD	0.003	0.005	–0.024	–0.041	0.025	0.041
	BWD	0.002	0.004	–0.025	–0.028	0.025	0.028
TH-1 01	FWD	0.000	0.002	–0.015	–0.031	0.015	0.029
	NAD	0.000	0.004	–0.004	–0.062	0.004	0.066
	BWD	0.001	0.002	–0.054	–0.032	0.048	0.030
TH-1 02	FWD	0.000	0.000	–0.018	–0.021	0.019	0.021
	NAD	0.000	0.000	–0.009	–0.006	0.009	0.007
	BWD	0.001	0.000	–0.053	–0.044	0.050	0.044
WV_2		0.001	0.003	–0.011	–0.039	0.010	0.046
Pleiades		0.000	0.000	–0.001	–0.008	0.001	0.007

The object coordinates of these points on three elevation planes are calculated by RPCs, and a total of 30 603 checkpoints are obtained. The image coordinates of these points are calculated by EGSM and compared with known coordinates. The statistical results of RMSE, minimum, and maximum differences are shown in Table III.

The results show that EGSM can be completely recovered from RPCs with residuals smaller than 0.1 pixels. The results show also that the effect of the IO parameters inaccuracy can be well compensated by the EO parameters and that the residuals of polynomials fitting of projection centers can be eliminated by the sensor rotation. That is evidence of the high correlation between the orientation parameters. The weakness in the geometric configuration of HRSI increases the robustness of the reconstruction process against inaccurate knowledge of the internal characteristics of the satellite sensors [13]. The feasibility

TABLE IV
EGSM-BASED BLOCK ADJUSTMENT RESULTS OF ZY-3 IMAGES (UNIT: M)

Number of GCPs	Mean error			Standard deviation				RMSE	
	X	Y	Z	X	Y	XY	Z	XY	Z
0	0.1	11.2	7.9	2.0	1.5	2.5	2.0	11.4	8.1
1	–0.8	–1.2	1.1	1.9	1.5	2.4	2.0	2.8	2.3
4	1.8	–0.3	–1.0	1.9	1.2	2.3	1.4	2.9	1.8
5	1.3	–0.5	–0.6	1.9	1.2	2.3	1.4	2.6	1.5
8	0.5	–0.1	–0.5	1.9	1.2	2.2	1.5	2.3	1.5
9	0.4	–0.3	–0.3	1.9	1.2	2.2	1.4	2.3	1.5
19	–0.1	0.0	0.0	1.8	1.1	2.2	1.3	2.2	1.3

of the proposed step-by-step approach for EGSM recovery from RPCs is verified.

In this experiment, the fourth-order Chebyshev polynomials are used for orbit fitting. In total, there are 26 parameters for an EGSM recovered from the RPCs of a satellite image. It is noteworthy that as an equivalent form of RFMs, EGSMs represent the relationship of the point coordinates in the imagery and object space with much fewer parameters than RFMs do. Furthermore, these parameters can be updated within a block adjustment to compensate for nonlinear systematic errors of the images. The initial value of the EGSM parameters can be fully recovered by the virtual lines of sight obtained from RPCs, while the image distortions or nonlinear systematic errors of the imagery do not affect the EGSM recovery because the real imagery is not used in the process.

B. Self-Calibration Block Adjustment Based on EGSM

1) Block Adjustment of Multiple ZY-3 Images: The experimental data (images, tie points, and GCPs) described in Section III are used. Block adjustments based on EGSM are carried out with different numbers of GCPs. The mean error and standard deviation of GCPs' coordinate residuals are shown in Table IV.

Similar to the results of RFM-based block adjustment, the main factors affecting positioning accuracy without GCPs are shifts in the Y and Z direction. When one control point is used to eliminate the offsets, the absolute positioning accuracy is greatly improved. When more control points are used, the standard deviation is reduced but not significantly. Fig. 8 shows a comparison between the accuracy of RFM-based and that of EGSM-based block adjustments with different numbers of GCPs. In terms of the horizontal accuracy, when the number of control points is less (<8 for the test data), the EGSM-based adjustment is significantly better than the RFM-based adjustment, and when the control points reach a certain number, the accuracy remains the same; in terms of the vertical accuracy, the results of EGSM-based adjustment are always better than those of RFM-based adjustment with a different number of control points. The experimental results show the following.

1) As an equivalent form of RSMs, the EGSM properly reflects the reality of sensor geometry and corrects the nonlinear systematic errors caused by attitude vibrations and other local distortions. Compared with RFMs, the EGSM-based block adjustments of multiview satellite images produce results of better accuracy (in terms of standard deviation) with fewer GCPs or even without GCPs. This is consistent with the conclusions of previous studies [12]–[14].
2) Due to imperfect sensor calibration or other reasons, there are obvious affine distortions on ZY-3 images. The linear distortions can be substantially compensated with four

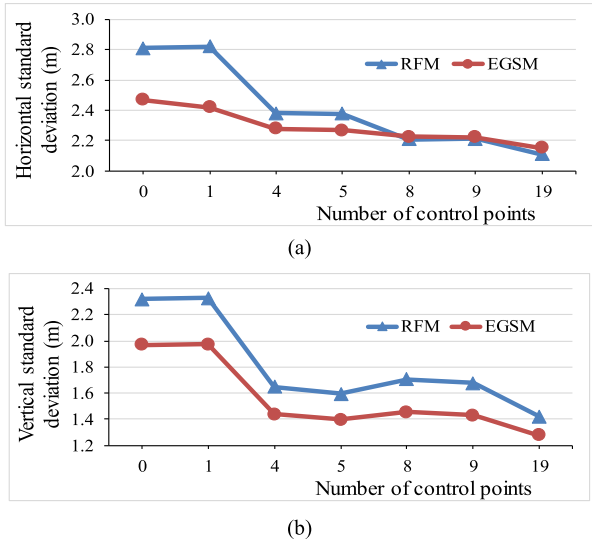

Fig. 8. Accuracy comparison of block adjustments based on RFM and EGSM with 12 stereo scenes ZY-3 satellite images: comparison of (a) horizontal and (b) vertical accuracies after adjustment.

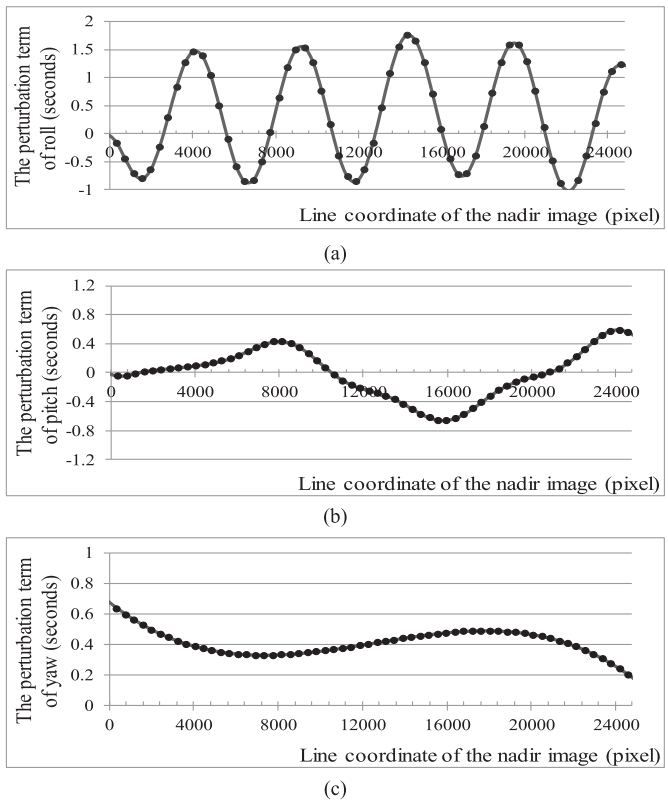

Fig. 9. Sensor attitude perturbation polynomials: the relation between the perturbation terms of (a) roll, (b) pitch, and (c) yaw and the line coordinate of the nadir image.

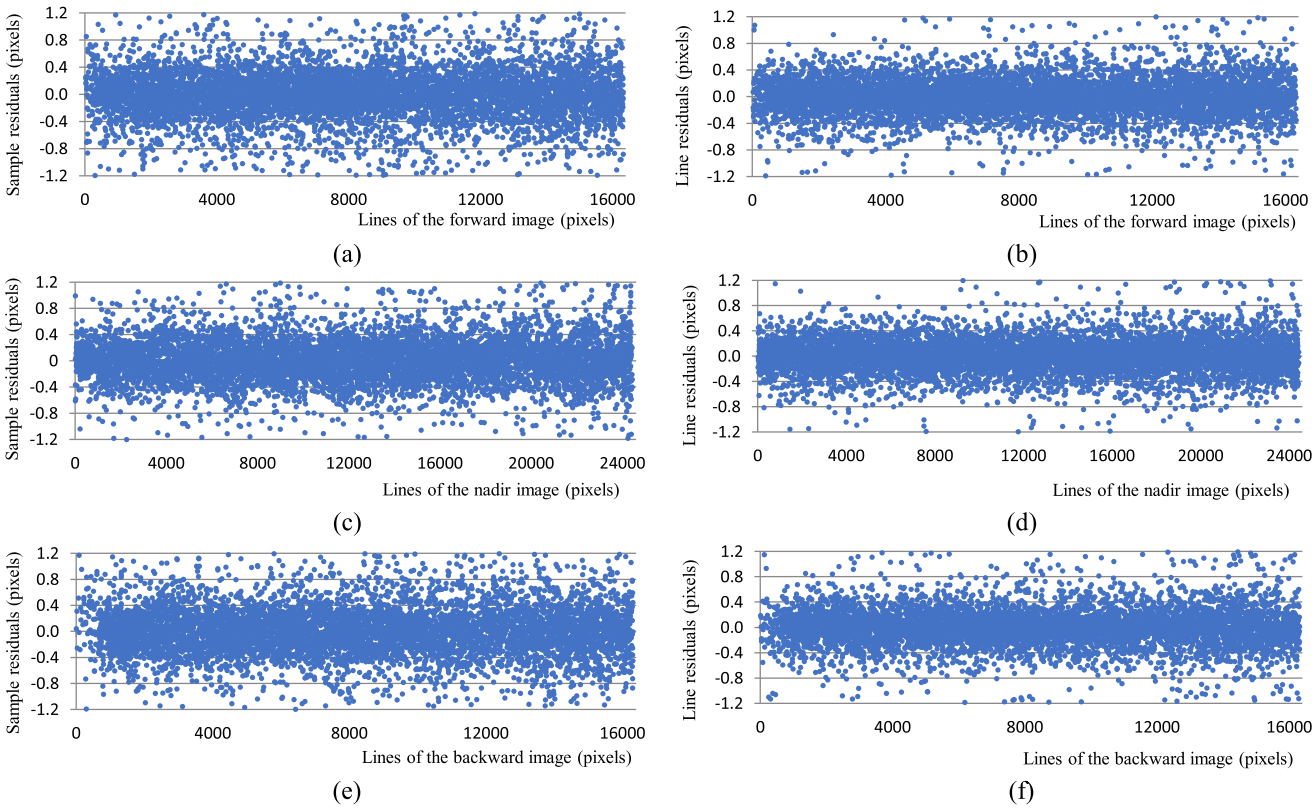

Fig. 10. Image point residuals of block adjustment based on EGSM (unit: pixel): (a) $\boldsymbol{v_s}$ and (b) $\boldsymbol{v_l}$ with respect to the line of the forward image, (c) $\boldsymbol{v_s}$ and (d) $\boldsymbol{v_l}$ with respect to the line of the nadir image, (e) $\boldsymbol{v_s}$ and (f) $\boldsymbol{v_l}$ with respect to the line of the backward image.

well-distributed GCPs by the block adjustment based on EGSM or the RFM method based on an affine transformation. When four GCPs are used, the accuracy of the object coordinates is improved significantly for both EGSM and RFM-based results.

3) When more than four GCPs are used, the standard deviations change only slightly as all unknowns of the block adjustment are treated as pseudo observations in the implementation of this study. This implementation reduces the influence of GCPs on the results since GCPs are also used as pseudo observations. When eight or nine GCPs are used, the standard deviations of the height increase by 0.1 m (about 0.05 pixels). The reason for this might be an inappropriate configuration of the pseudo observations' weights, which are determined according to the a posteriori variance estimations. This should be further investigated with more experimental datasets.
4) When the number of control points is greater than 5, there is little difference between the planimetric standard deviations of EGSM and RFM. It does not mean the performance of RFM is similar to EGSM in these cases because obvious systematic errors in the residuals of the image coordinates exist as shown in Section III. A statistical analysis of the residuals of image coordinates has to be conducted.

2) Compensation for Systematic Errors: Self-calibration for nonlinear systematic error compensation is applied in block adjustment based on EGSM. And the additional parameters are automatically calculated during the adjustment. The linear array CCD deformation is effectively corrected and the image point residuals are not systematically distributed along the scan line direction. Since the satellite attitude perturbation is expressed in the EGSM, the image distortions caused by the attitude vibration can be effectively compensated in EGSM-based block adjustment.

The distribution of image point residuals corresponding to the same scene of Fig. 3 is shown in Fig. 10. The systematic oscillation is effectively eliminated. Fig. 9(a), (b), and (c) show the perturbation terms (the nonlinear terms of the polynomials) of attitude roll, pitch, and yaw of the nadir image solved in block adjustment based on EGSM corresponding to the image point residuals shown in Figs. 3 and 10. The x-axis is the image line coordinate, and the y-axis is the perturbation value of the attitude angle (in the unit of seconds). The roll angle disturbance term exhibits obvious periodicity, with a period of about 5025 pixels and a vibration range of about $2.6''$ (the satellite orbital height of ZY-3 is approximately 506 km, the GSD of the nadir image is about 2.1 m, and $2.6''$ of the roll is equivalent to 3.04 pixels), which is in line with the residuals v_s of the nadir image shown in Fig. 3. The curve of the pitch angle disturbance term is in the same shape as that of v_l. of the nadir image shown in Fig. 3 too. Therefore, the attitude disturbance term in block adjustment based on EGSM fully reflects the systematic image point residuals caused by jitters and effectively corrects for it.

With the adjusted EGSM orientation parameters, the object coordinates of the tie points are calculated by the forward intersection for each stereo scene and then are compared with the coordinates of the block adjustment results. The coordinate

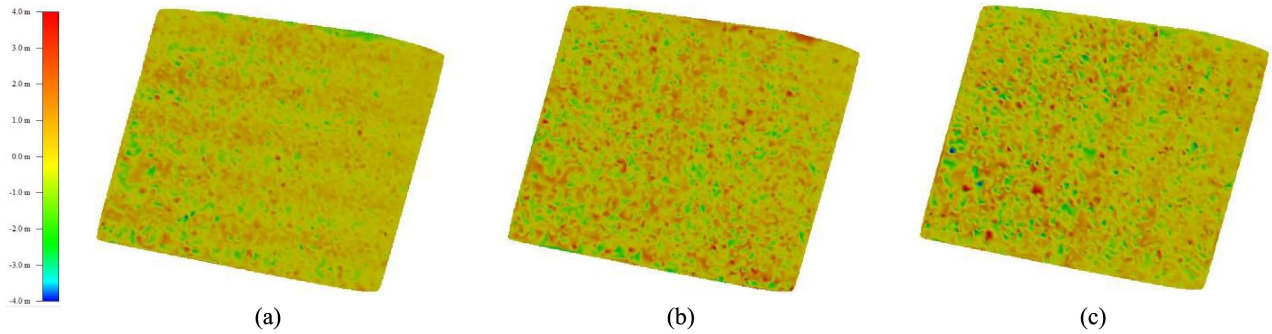

Fig. 11. Differences of ground coordinates between the stereo model intersection and EGSM-based block adjustment: residuals in the directions of (a) east-west (longitude), (b) north-south (latitude), and (c) height.

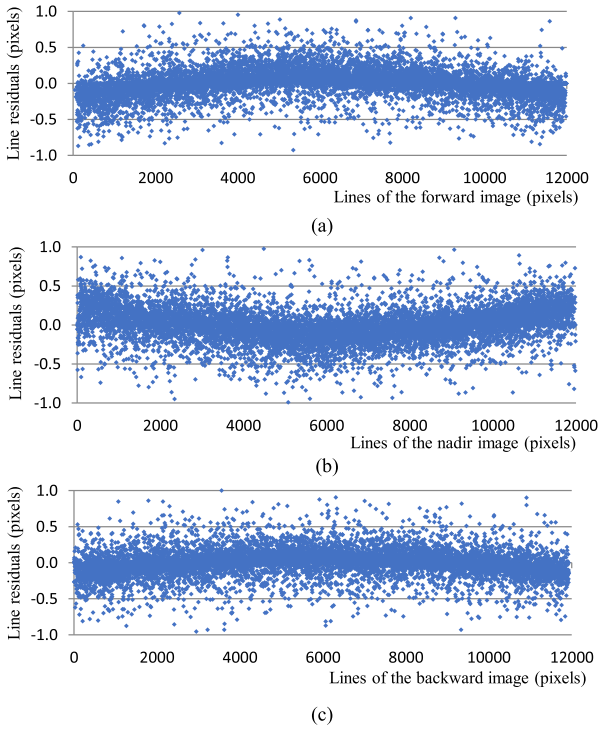

Fig. 12. Residuals undulation of the RFM-based block adjustment of the TH-1 test images (unit: pixel): the line coordinate residuals of (a) forward, (b) nadir, and (c) backward imagery along its imagery lines.

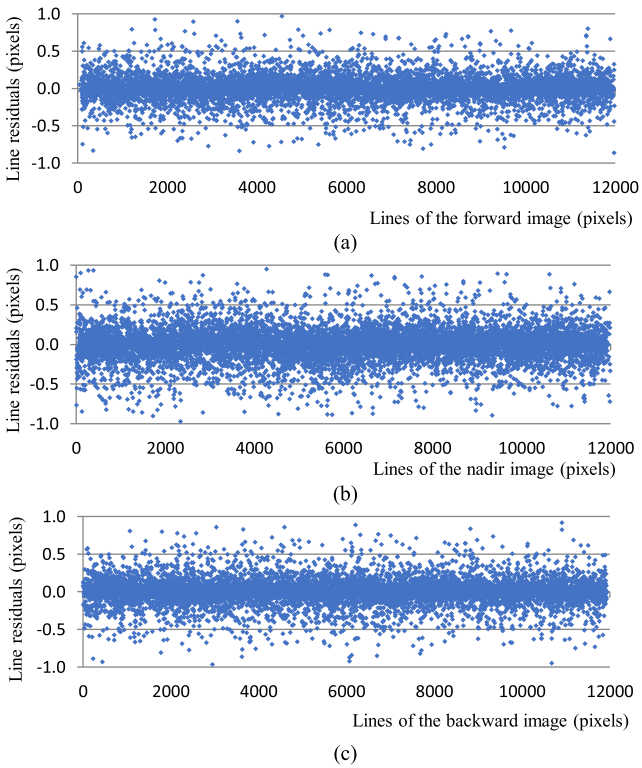

Fig. 13. Residuals of image coordinates of the EGSM-based block adjustment of the TH-1 test images (unit: pixel): the line coordinate residuals of (a) forward, (b) nadir, and (c) backward imagery along its imagery lines.

differences of longitude, latitude, and height of the stereo scene in the upper right corner of the region are shown in Fig. 11. The experimental results show that the EGSM-based block adjustment can effectively compensate for the local distortions and that there are no obvious systematic errors in the coordinates obtained from the forward intersection of the stereo model. Compared with the results shown in Fig. 4, the strip-wise systematic errors are effectively eliminated.

The experimental results demonstrate the following advantages of the proposed EGSM-based approach compared with other methods for nonlinear bias compensation of ZY-3 images.

1) The EGSM-based self-calibration block adjustment can completely compensate for the local image distortions caused by attitude vibration, deformations of CCD sensors, and other uncalibrated errors. In other words, the compensation for the periodic distortions caused by attitude oscillation in the across-track direction [4] or for the residual errors of the RPC's generation [5] is not the only case that the EGSM method can be applied to.
2) An EGSM of satellite imagery can be established by only the associated RPCs. The EGSM-based self-calibration block adjustment can be conducted with very few or even without GCPs. Other methods require either the metadata to establish RSMs of the images [5], or more well-distributed GCPs to get better results [30].

3) Block Adjustment of TH-1 Images: To further show the feasibility of the proposed method and prove the generalization ability of the proposed method, a set of TH-1 images is used for experiments. The two stereo scenes (consisted of forward,

nadir, and backward images) of TH-1 images are located within the test region of Fig. 1 and overlaid on each other. They are captured in September 2015 and March 2016, respectively.

Approximately 14 700 tie points are automatically extracted by multilevel image matching and there are about 9500 points per image. More than 60% of the tie points are located in four or more images. And about 13 700 of the tie-points are transferred to the ZY-3 images also. RFM-based block adjustments with a set of affine transformation parameters in the image space for bias compensation are carried out. The adjusted ground coordinates of the tie-points are compared with the results from the ZY-3 images described in the last section. It seems that the terrain heights from the TH-1 images are inclined on both along-track and across-track directions. The image coordinates residuals of the images captured in March 2016 are shown in Fig. 12. The nonlinear systematic errors can be easily identified. The residuals of EGSM-based block adjustment are presented in Fig. 13. The systematic errors are well eliminated there.

VII. Conclusion

In this article, the recovery of the EGSM from RPCs is discussed in detail. The EGSM-based self-calibration block adjustment of satellite images and the RPCs optimization are presented. The experimental results verify the effectiveness of the proposed algorithm and its suitability for the geometric processing of HRSI from various satellites. The effectiveness is also demonstrated that an EGSM is used as an equivalent form of the RFM in the absence of metadata related to platforms and sensors. Experiments show the following.

The various error sources of satellite images can be well analyzed and modeled in the EGSM-based block adjustment. Self-calibration block adjustment based on EGSM can effectively eliminate the nonlinear systematic errors in satellite images and the associated RPCs. The geometric interpretation of EGSM parameters is so obvious that prior knowledge of the satellite and sensor can be introduced as constraints or virtual observations in the block adjustment process.

The EGSM parameters, including equivalent focal length, principal point coordinate, the instantaneous position of the projection center of the scan line, and the corresponding attitude rotation matrix, can be directly solved from RPCs. An EGSM can be completely established by only the RPCs of a satellite image with residuals smaller than 0.1 pixels without using any metadata relating to satellite ephemeris, attitude measurements, and sensor parameters. The local distortions of the imagery do not affect the EGSM parameter recovery because the process is using only virtual points obtained from the RPCs but not the real imagery.

The optimized RPCs of satellite images can be regenerated from the EGSM. The correction grids can be used for satellite image resampling or image point coordinates correction in RFM applications, thus effectively eliminating system errors in the original RPCs.

Because more unknowns are introduced in the block adjustment, the computation costs of the EGSM-based approach are higher than RFM in terms of complexity and time. To avoid excessive parameterization and reduce the correlation between parameters, a set of appropriate inner constraints and pseudo observations should be used in the self-calibration block adjustment. This needs to be further investigated. The comparisons with other methods will add value and should be further investigated too.

Acknowledgment

The authors would like to thank the China Centre for Resources Satellite Data and Application (CRESDA) and Airbus for providing the ZY-3 images and Melbourne dataset of Pleiades images for the test, respectively.

References

[1] V. Amberg, C. Dechoz, L. Lebegue, D. Greslou, F. de Lussy, and L. Lebegue, "In-flight attitude perturbances estimation: Application to PLEIADES-HR satellites," in *Proc. SPIE*, San Diego, CA, USA, 2013, Art. no. 886612.

[2] K. Jacobsen, "Problems and limitations of satellite image orientation for determination of height models," in *Proc. Int. Arch. Photogrammetry, Remote Sens. Spatial Inf. Sci.- ISPRS Arch. 42(W1)*, Hannover, Germany, 2017, pp. 257–264.

[3] T. Sun, H. Long, B. Liu, and Y. Li, "Application of attitude jitter detection based on short-time asynchronous images and compensation methods for Chinese mapping satellite-1," *Opt. Exp.*, vol. 23, no. 2, pp. 1395–1410, Jan. 2015.

[4] X. Tong *et al.*, "Detection and estimation of ZY-3 three-line array image distortions caused by attitude oscillation," *ISPRS J. Photogrammetry Remote Sens.*, vol. 101, pp. 291–309, Mar. 2015.

[5] J. Cao, J. Fu, X. Yuan, and J. Gong, "Nonlinear bias compensation of Ziyuan-3 satellite imagery with cubic splines," *ISPRS J. Photogrammetry Remote Sens.*, vol. 133, pp. 174–185, Nov. 2017.

[6] M. Wang, C. Fan, J. Pan, S. Jin, and X. Chang, "Image jitter detection and compensation using a high-frequency angular displacement method for Yaogan-26 remote sensing satellite," *ISPRS J. Photogrammetry Remote Sens.*, vol. 130, pp. 32–43, Aug. 2017.

[7] T. Toutin, "Review article: Geometric processing of remote sensing images: Models, algorithms and methods," *Int. J. Remote Sens.*, vol. 25, no. 10, pp. 1893–1924, May 2004.

[8] C. S. Fraser, G. Dial, and J. Grodeki, "Sensor orientation via RPCs," *ISPRS J. Photogrammetry Remote Sens.*, vol. 60, pp. 182–194, May 2006.

[9] T. Kim and I. Dowman, "Comparison of two physical sensor models for satellite images: Position-rotation model and orbit-attitude model," *Photogrammetric Rec.*, vol. 21, pp. 110–123, Jun. 2006.

[10] D. Poli and T. Toutin, "Review of developments in geometric modelling for high resolution satellite pushbroom sensors," *Photogrammetric Rec.*, vol. 27, no. 137, pp. 58–73, Mar. 2012.

[11] J. Jeong and T. Kim, "Comparison of positioning accuracy of a rigorous sensor model and two rational function models for weak stereo geometry," *ISPRS J. Photogrammetry Remote Sens.*, vol. 108, pp. 172–182, Oct. 2015.

[12] T. Toutin, "Spatiotriangulation with multisensor HR stereo-images," *IEEE Trans. Geosci. Remote Sens.*, vol. 44, no. 2, pp. 456–462, Feb. 2006.

[13] A. Habib *et al.*, "Comprehensive analysis of sensor modeling alternatives for high resolution imaging satellites," *Photogrammetric Eng. Remote Sens.*, vol. 73, no. 11, pp. 1241–1251, Nov. 2007.

[14] D. Poli, "A rigorous model for spaceborne linear array sensors," *Photogrammetric Eng. Remote Sens.*, vol. 73, no. 2, pp. 187–196, Feb. 2007.

[15] C. V. Tao and Y. Hu, "A comprehensive study of the rational function model for photogrammetric processing," *Photogrammetric Eng. Remote Sens.*, vol. 67, no. 12, pp. 1347–1357, Dec. 2001.

[16] J. Oh and C. Lee, "Automated bias-compensation of rational polynomial coefficients of high resolution satellite imagery based on topographic maps," *ISPRS J. Photogrammetry Remote Sens.*, vol. 100, pp. 14–22, Feb. 2015.

[17] Y. Jiang, G. Zhang, P. Chen, D. Li, X. Tang, and W. Huang, "Systematic error compensation based on a rational function model for Ziyuan1-02C," *IEEE Trans. Geosci. Remote Sens.*, vol. 53, no. 7, pp. 3985–3995, Jul. 2015.

[18] Y. Zhang, Y. Lu, L. Wang, and X. Huang, "A new approach on optimization of the rational function model of high-resolution satellite imagery," *IEEE Trans. Geosci. Remote Sens.*, vol. 50, no. 7, pp. 2758–2764, Jul. 2012.
[19] T. Long, W. Jiao, and G. He, "RPC estimation via L1-norm-regularized least squares (L1LS)," *IEEE Trans. Geosci. Remote Sens.*, vol. 53, no. 8, pp. 4554–4567, Aug. 2015.
[20] S. Gholinejad, A. Amiri-Simkooei, S. Moghaddam, and A. Naeini, "An automated PCA-based approach towards optimization of the rational function model," *ISPRS J. Photogrammetry Remote Sens.*, vol. 165, pp. 133–139, Jul. 2020.
[21] H. Cao, P. Tao, H. Li, and J. Shi, "Bundle adjustment of satellite images based on an equivalent geometric sensor model with digital elevation model," *ISPRS J. Photogrammetry Remote Sens.*, vol. 156, pp. 169–183, Oct. 2019.
[22] Y. Hu and C. V. Tao, "Updating solutions of the rational function model using additional control information," *Photogrammetric Eng. Remote Sens.*, vol. 68, no. 7, pp. 715–723, Jul. 2002.
[23] J. Grodecki and G. Dial, "Block adjustment of high-resolution satellite images described by rational polynomials," *Photogrammetric Eng. Remote Sens.*, vol. 69, no. 1, pp. 59–68, Jan. 2003.
[24] K. Di, R. Ma, and R. Li, "Rational functions and potential for rigorous sensor model recovery," *Photogrammetric Eng. Remote Sens.*, vol. 60, no. 1, pp. 33–41, Jan. 2003.
[25] Z. Xiong and Y. Zhang, "A generic method for RPC refinement using ground control information," *Photogrammetric Eng. Remote Sens.*, vol. 79, no. 9, pp. 1083–1092, Sep. 2009.
[26] Z. Xiong and Y. Zhang, "Bundle adjustment with rational polynomial camera models based on generic method," *IEEE Trans. Geosci. Remote Sens.*, vol. 49, no. 1, pp. 190–202, Jan. 2011.
[27] W. Huang, G. Zhang, X. Tang, and D. Li, "Compensation for distortion of basic satellite images based on rational function model," *IEEE J. Sel. Topics Appl. Earth Observation Remote Sens.*, vol. 9, no. 12, pp. 5767–5775, Dec. 2016.
[28] C. Li *et al.*, "An improved geopositioning model of quickbird high resolution satellite imagery by compensating spatial correlated errors," *ISPRS J. Photogrammetry Remote Sens.*, vol. 96, pp. 12–19, Oct. 2014.
[29] X. Tong, S. Liu, and Q. Weng, "Bias-corrected rational polynomial coefficients for high accuracy geo-positioning of quickbird stereo imagery," *ISPRS J. Photogrammetry Remote Sens.*, vol. 65, pp. 218–226, Mar. 2010.
[30] X. Shen, B. Liu, and Q. Li, "Correcting bias in the rational polynomial coefficients of satellite imagery using thin-plate smoothing splines," *ISPRS J. Photogrammetry Remote Sens.*, vol. 125, pp. 125–131, Mar. 2017.
[31] J. Wertz, *Spacecraft Attitude Determination and Control*. Dordrecht, The Netherlands: Springer, 1987.
[32] X. Ren *et al.*, "A global adjustment method for photogrammetric processing of Chang'E-2 stereo images," *IEEE Trans. Geosci. Remote Sens.*, vol. 57, no. 9, pp. 6832–6843, Sep. 2019.
[33] M. Mazaheri and A. Habib, "Quaternion-based solutions for the single photo resection problem," *Photogrammetric Eng. Remote Sens.*, vol. 81, no. 3, pp. 209–217, Mar. 2015.
[34] Astrium Inc., "Pleiades imagery user guide," Oct. 2012 –v2.0. [Online]. Available: https://www.intelligence-airbusds.com/docs/
[35] F. de Lussy, P. Kubik, D. Greslou, V. Pascal, P. Gigord, and J. P. Cantou, "Pleiades-HR image system products and geometric accuracy," in *Proc. Int. Soc. Photogrammetry Remote Sens. Int. Conf.*, Hannover, Germany, 2005, pp. 17–20.

Hui Cao received the B.S. and M.S. degrees in photogrammetry from Wuhan Technical University of Surveying and Mapping, Wuhan, China, in 1985 and 1996, respectively, and the Ph.D. degree in photogrammetry and remote sensing from Wuhan University, Wuhan, China, in 2013.

He is currently an Associate Professor of Photogrammetry and Remote Sensing with the School of Remote Sensing and Information Engineering, Wuhan University. His research interests include satellite and aerial photogrammetry, image matching, change detection, and 3-D city reconstruction.

Pengjie Tao received the B.S. degree in remote sensing science and technology, and the Ph.D. degree in photogrammetry and remote sensing from Wuhan University, Wuhan, China, in 2008 and 2016, respectively.

He is currently an Associate Research Fellow with the School of Remote Sensing and Information Engineering, Wuhan University. His research interests include satellite images photogrammetry, registration of optical images and LiDAR points, and multiview images 3-D reconstruction.

Yuxuan Liu received the M.S. degree in surveying and mapping engineering from Information Engineering University, Zhengzhou, China, in 2016, and the Ph.D. degree in photogrammetry and remote sensing from the School of Remote Sensing and Information Engineering, Wuhan University, Wuhan, China, in 2020.

He is currently a Research Associate with the Chinese Academy of Surveying and Mapping. His research interests include image matching, light fields, and 3-D reconstruction from images and point clouds.

Haihong Li received the B.S. and M.S. degrees in photogrammetry and remote sensing from the Wuhan Technical University of Surveying and Mapping, Wuhan, China, in 1984 and 1987, respectively, and the Ph.D. degree in photogrammetry and remote sensing from the Institute of Geodesy and Photogrammetry, Swiss Federal Institute of Technology (ETHZ), Zürich, Switzerland, in 1996.

His research interests include satellite image processing, sensor modeling, lunar mapping, integration of multisource data, and location-based service.